Supporting Information

Modulating interfacial electric field in oxygen-defect-mediated S-scheme Mo-$ZnIn_2S_4$/BiOCl heterostructures for efficient photocatalytic hydrogen evolution

Jinyu Wang, Jiafeng Zhu, Jiacheng Zhang, Hong Li, Qingyuan Bi, Jinchen Fan, Zichao Lian*, Guisheng Li*

School of Materials and Chemistry, University of Shanghai for Science and Technology, Shanghai 200093, P. R. China

***Corresponding Author:** zichaolian@usst.edu.cn; liguisheng@usst.edu.cn

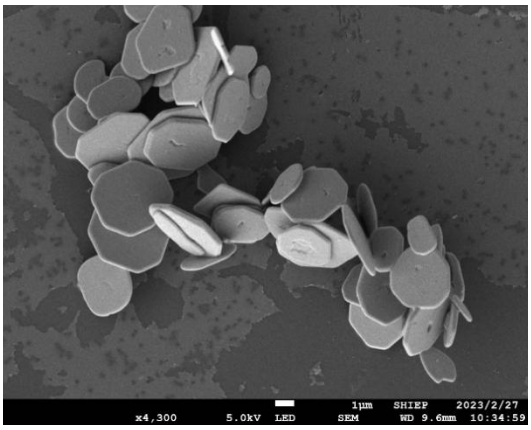

Fig. S1. SEM image of BOC.

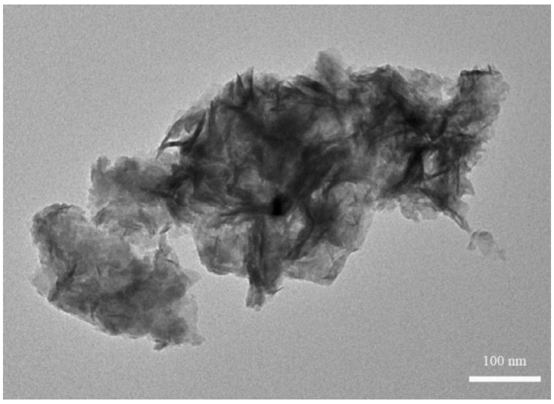

Fig. S2. TEM image of $Mo_{0.5}$-ZIS.

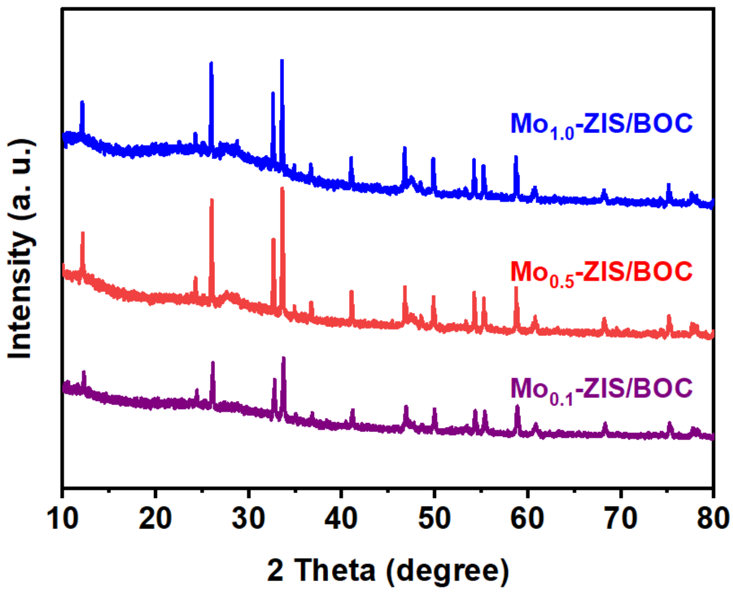

Fig. S3. XRD patterns of $Mo_{0.1}$-ZIS/BOC, $Mo_{0.5}$-ZIS/BOC and $Mo_{1.0}$-ZIS/BOC.

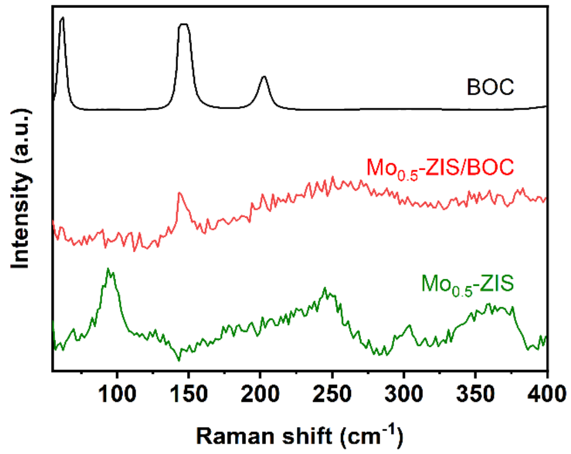

Fig. S4. Raman spectra of BOC, $Mo_{0.5}$-ZIS, and $Mo_{0.5}$-ZIS/BOC.

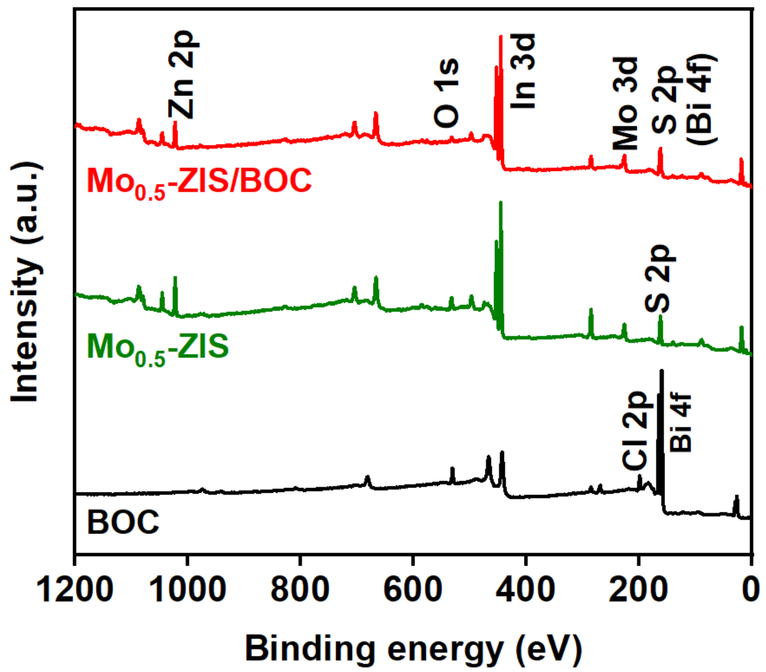

Fig. S5. XPS survey spectra of BOC, $Mo_{0.5}$-ZIS and $Mo_{0.5}$-ZIS/BOC.

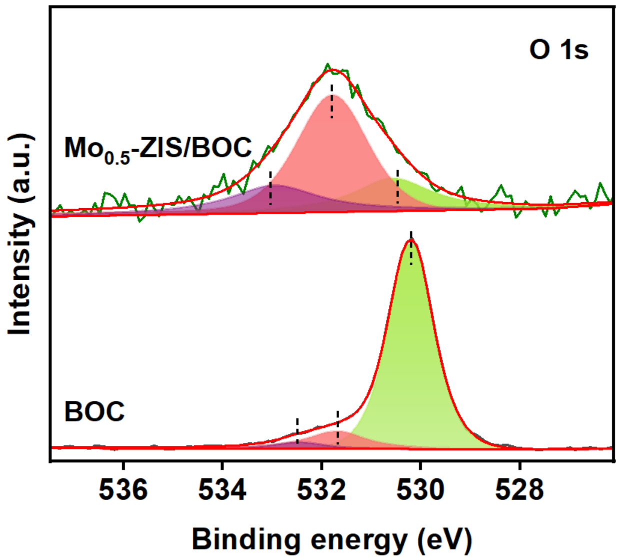

Fig. S6. High-resolution XPS spectra of O1s.

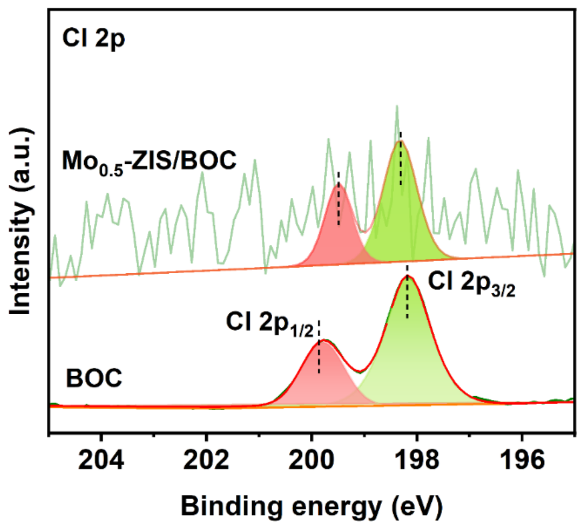

Fig. S7. High-resolution XPS spectra of Cl 2p.

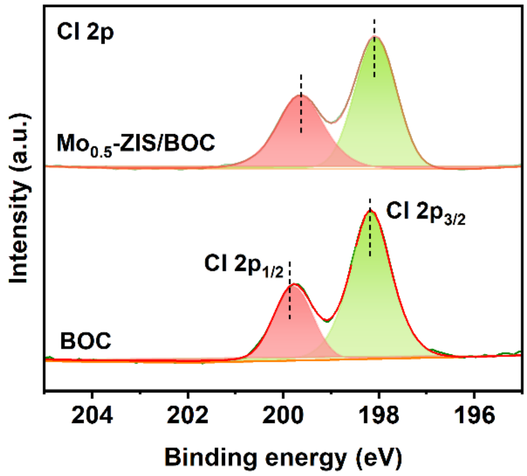

Fig. S8. High-resolution XPS spectra of Cl 2p (the BOC in $Mo_{0.5}$-ZIS/BOC with higher content).

Note: The Cl signal in the XPS spectrum of $Mo_{0.5}$-ZIS/BOC is weak. To better understand the variation in the electron binding energy of Cl, we tested the $Mo_{0.5}$-ZIS/BOC sample with a higher Cl content, in which the amount of BOC was 200 mg.

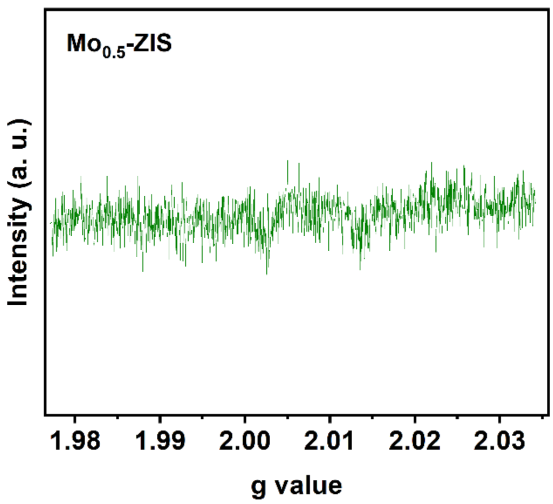

Fig. S9. EPR spectroscopy of $Mo_{0.5}$-ZIS.

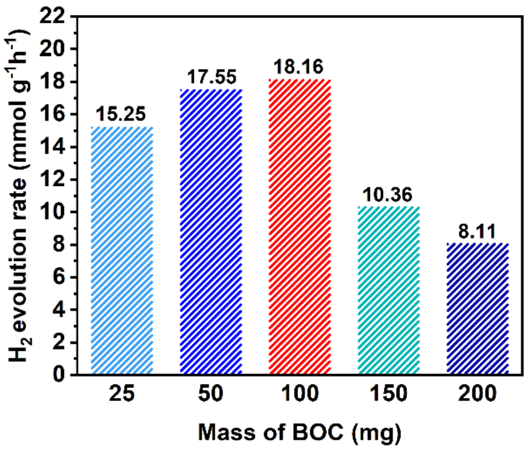

Fig. S10. Effect of BOC mass fraction in $Mo_{0.5}$-ZIS/BOC on hydrogen evolution performance.

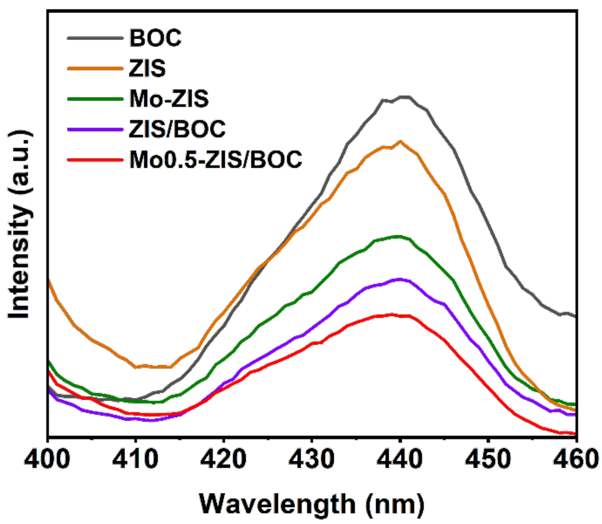

Fig. S11. Steady-state PL spectra of the photocatalysts.

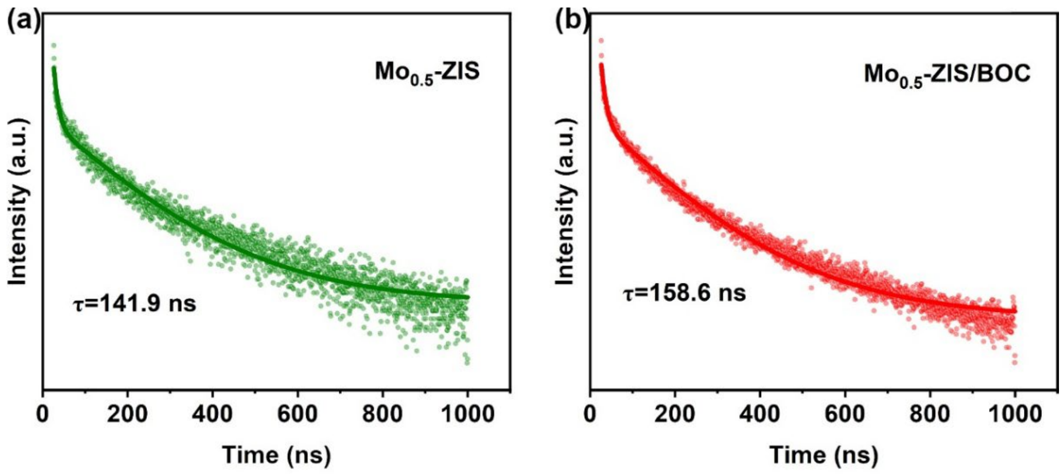

Fig. S12. TRPL spectra of $Mo_{0.5}$-ZIS and $Mo_{0.5}$-ZIS/BOC.

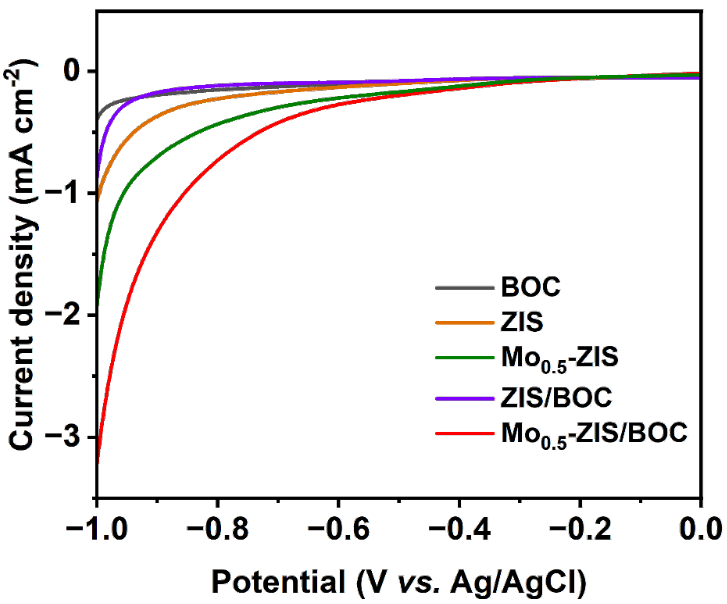

Fig. S13. LSV curves of the photocatalysts.

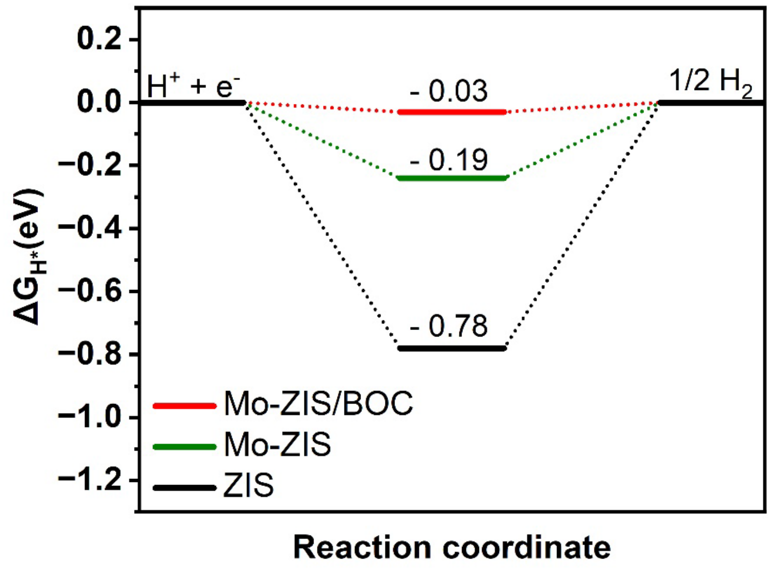

Fig. S14. Hydrogen absorption free energy of ZIS, Mo-ZIS, and Mo-ZIS/BOC.

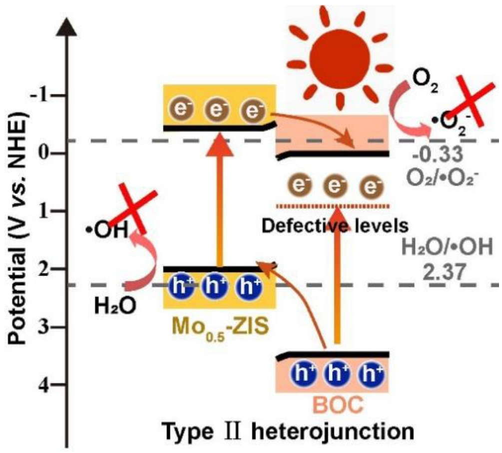

Fig. S15. Type II charge carrier transfer mechanism for $Mo_{0.5}$-ZIS/BOC heterojunction.

Table S1. Comparison of representative $ZnIn_2S_4$-based photocatalysts for H_2 evolution efficiency.

Photocatalysts	**Light source**	**H_2 evolution rate (mmol g^{-1} h^{-1})**	**AQY**	**Ref.**
Zr-MOF@$ZnIn_2S_4$	300 W Xe lamp (> 400 nm)	8.53	4.1% (420 nm)	[1]
ZnO/UiO-66-NH_2/$ZnIn_2S_4$	300 W Xe lamp (> 400 nm)	5.05	1.62% (420 nm)	[2]
(CuNiFe)M-C-$ZnIn_2S_4$	500 W Xe lamp (320 nm-2500 nm)	6.5	-	[3]
$ZnIn_2S_4$/Au/$Cd_{0.7}Zn_{0.3}S$	300 W Xe lamp (320 nm-2500 nm)	4.57	-	[4]
PdS-$ZnIn_2S_4$	300 W Xe lamp (> 420 nm)	0.615	0.4% (420 nm)	[5]
$ZnIn_2S_4$/$CuCo_2S_4$	300 W Xe lamp (320 nm-2500 nm)	6.24	26.44% (400 nm)	[6]
$ZnIn_2S_4$/O-$ZnIn_2S_4$	300 W Xe lamp (> 400 nm)	7.145	1.75% (420 nm)	[7]
$ZnIn_2S_4$/CeO_2	300 W Xe lamp (> 420 nm)	3.29	9.7% (405 nm)	[8]
ReS_2/$ZnIn_2S_4$	LED (420 nm)	2.24	11.32% (420 nm)	[9]
Pt-$ZnIn_2S_4$	300 W Xe lamp (> 420 nm)	8.27	53.5% (420 nm)	[10]
N-$ZnIn_2S_4$	350 W Xe lamp (> 400 nm)	1.575	6.59% (420 nm)	[11]
POM-$ZnIn_2S_4$	300 W Xe lamp (> 420 nm)	10.6	18.8% (420 nm)	[12]
COF/$ZnIn_2S_4$	300 W Xe lamp (> 420 nm)	2.3	5.02% (420 nm)	[13]
$ZnIn_2S_4$/CdS	300 W Xe lamp (> 420 nm)	7.4	12.6% (420 nm)	[14]

MoS_2/O-$ZnIn_2S_4$	300 W Xe lamp (> 420 nm)	4	2.53% (nm)	[15]
$FeNi_2S_4$/$ZnIn_2S_4$	300 W Xe lamp (320 nm-2500 nm)	7.7	17.35% (420 nm)	[16]
1-Pt/$ZnIn_2S_4$	300 W Xe lamp (320 nm-2500 nm)	12.29	10.5% (400 nm)	[17]
Nickel porphyrin/$ZnIn_2S_4$	300 W Xe lamp (> 400 nm)	2.305	64% (400 nm)	[18]
$ZnIn_2S_4$/WO_3	300 W Xe lamp (> 420 nm)	2.6	0.13% (420 nm)	[19]
$Mo_{0.5}$-ZIS/BOC	300 W Xe lamp (> 420 nm)	18.16	23.3% (420 nm)	This work

Supplementary references:

[1] L. Liu, L. Zuo, X. Zhai, X. Xiao, H. Fan, B. Li, L. Wang, A novel hexagonal prism of Zr-based MOF@$ZnIn_2S_4$ core-shell nanorod as an efficient photocatalyst for hydrogen evolution, Appl. Catal., B, 2025, **361**, 124686.

[2] X. Xiao, S. Li, L. Zuo, R. Li, Z. Li, L. Liu, H. Fan, B. Li, Twin S-scheme heterojunction ZnO/UiO-66-NH_2@$ZnIn_2S_4$ rhombic octahedra for efficient photocatalytic H_2 evolution, Adv. Funct. Mater., 2025, 2418778.

[3] J. Zhang, L. Hu, E. Wu, B. Qian, S.S.A. Shuaib, J. Wang, M. Cai, J. Bai, Y. Jiang, J. Chen, C. Mao, S. Sun, CuNiFe alloy-modified MWCNTs derived from waste battery leachate for enhanced photocatalytic H_2 evolution over $ZnIn_2S_4$, Adv. Funct. Mater., 2025, 2504286.

[4] X. Sun, J. Zhang, M. Luo, J. Ma, T. Xian, G. Liu, H. Yang, Elevating photocatalytic H_2 evolution over $ZnIn_2S_4$@Au@$Cd_{0.7}Zn_{0.3}S$ multilayer nanotubes via Au-mediating H–S antibonding-orbital occupancy, Chem. Eng. J., 2024, **499**, 156455.

[5] X. Li, M. Qi, J. Li, C. Tan, Z. Tang, Y. Xu, Visible light-driven dehydrocoupling of thiols to disulfides and H_2 evolution over PdS-decorated $ZnIn_2S_4$ composites, Chin. J. Catal., 2023, **51**, 55-65.

[6] R. Wang, W. Yu, N. Fang, P. Wang, Y. Chu, S. Wu, J. Liang, Constructing fast charge separation of $ZnIn_2S_4$@$CuCo_2S_4$ p-n heterojunction for efficient photocatalytic hydrogen energy recovery from quinolone antibiotic wastewater, Appl. Catal., B, 2024, **341**, 123284.

[7] X. Li, Z. Su, S. Wu, L. Zheng, H. Zheng, L. Mao, X. Shi, Synergistic interactions of bulk polarization and built-in electric field inducing 2D/2D S-scheme homojunction toward enhanced photocatalytic performance, Small, 2024, **20**, 2406485.

[8] R. Jiang, L. Mao, Y. Zhao, J. Zhang, E.B. Chubenko, V. Bondarenko, Y. Sui, X. Gu, X. Cai, 1D/2D CeO_2/$ZnIn_2S_4$ Z-scheme heterojunction photocatalysts for efficient H_2 evolution under visible light, Sci. China Mater., 2023, **66**, 139-149.

[9] J. Xu, W. Zhong, F. Chen, X. Wang, H. Yu, *In-situ* cascade growth-induced strong coupling effect toward efficient photocatalytic hydrogen evolution of

$ReS_2/ZnIn_2S_4$, Appl. Catal., B, 2023, **328**, 122493.

[10] X. Shi, X. Wang, H. Jiang, X. Qin, X. Li, G. Sheng, C. Yu, L. Zheng, C. Zhu, L. Zheng, L. Mao, D. Ma, Y. Zhu, H. Zheng, Activating surface sulfur atoms via subsurface engineering toward boosted photocatalytic water splitting, Chem Catal., 2023, **3**, 100695.

[11] W.-K. Chong, B. Ng, X.Y. Kong, L. Tan, L.K. Putri, S. Chai, Non-metal doping induced dual p-n charge properties in a single $ZnIn_2S_4$ crystal structure provoking charge transfer behaviors and boosting photocatalytic hydrogen generation, Appl. Catal., B, 2023, **325**, 122372.

[12] F. Xing, R. Zeng, C. Cheng, Q. Liu, C. Huang, POM-incorporated $ZnIn_2S_4$ Z-scheme dual-functional photocatalysts for cooperative benzyl alcohol oxidation and H_2 evolution in aqueous solution, Appl. Catal., B, 2022, **306**, 121087.

[13] S. Bao, Q. Tan, S. Wang, J. Guo, K. Lv, S.A.C. Carabineiro, L. Wen, TpBD COF@$ZnIn_2S_4$ nanosheets: A novel S-scheme heterojunction with enhanced photoreactivity for hydrogen production, Appl. Catal., B, 2023, **330**, 122624.

[14] C. Li, X. Du, S. Jiang, Y. Liu, Z. Niu, Z. Liu, S. Yi, X. Yue, Constructing direct Z-scheme heterostructure by enwrapping $ZnIn_2S_4$ on CdS hollow cube for efficient photocatalytic H_2 generation, Adv. Sci., 2022, **9**, 2201773.

[15] Y. Peng, X. Guo, S. Xu, Y.n. Guo, D. Zhang, M. Wang, G. Wei, X. Yang, Z. Li, Y. Zhang, F. Tian, Surface modulation of MoS_2/O-$ZnIn_2S_4$ to boost photocatalytic H_2 evolution, J. Energy Chem., 2022, **75**, 276-284.

[16] S. Wang, D. Zhang, X. Pu, L. Zhang, D. Zhang, J. Jiang, Photothermal-enhanced S-scheme heterojunction of hollow core-shell $FeNi_2S_4$@$ZnIn_2S_4$ toward photocatalytic hydrogen evolution, Small, 2024, **20**, 2311504.

[17] S. Wu, X. Li, J. Liu, H. Wu, H. Xu, W. Bai, L. Mao, X. Shi, Effective photocatalytic ethanol reforming into high-value-added multicarbon compound coupled with H_2 production over Pt-S_3 sites at Pt_{SA}–$ZnIn_2S_4$ interface, Small, 2024, **20**, 2307386.

[18] H. Jia, X. Shao, Y.n. Wang, J. Zhang, R. Li, T. Peng, Nickel porphyrin/$ZnIn_2S_4$ heterojunction with Ni-S highway for boosting charge separation and visible-light-driven H_2 production, Appl. Catal., B, 2024, **353**, 124090.

[19] H. An, Y. Wang, X. Xiao, J. Liu, Z. Ma, T. Gao, W. Hong, L. Zhao, H. Wang, Q. Zhu, S. Chen, Z. Yin, Photocatalytic seawater splitting by 2D heterostructure of $ZnIn_2S_4/WO_3$ decorated with plasmonic Au for hydrogen evolution under visible light, J. Energy Chem., 2024, **93**, 55-63.